Journal of Applied Mechanics and Technical Physics, Vol. 49, No. 6, pp. 926–933, 2008

BORE IMPACT ON A VERTICAL PLATE

V. I. Bukreev and V. V. Zykov

UDC 532.532.+532.59

This paper describes the technique and results of an experimental study of the longitudinal force component, the vertical coordinate of its application point, and the overturning moment for the impact of a bore on a vertical plate. The bore was generated by removal of a shield which produced the initial free-surface level difference in the channel (in the model formulation of the dam-break problem). It is shown that the greatest forces and overturning moments occur at the ratio of the initial headwater and tailwater levels at which a bore with a developed head roller is formed.

Key words: *dam break, bore, vertical plate, drag force, overturning moment.*

Introduction. The term bore is used to refer to a moving hydraulic jump [1]. Waves of this type are produced by dam break, tsunami entering shallow water, high tidal waves entering a river, large bodies falling on shallow water, bank landslides, rapid stop of a container partially filled with a fluid, and other intense perturbations of fluid of finite depth. A review of studies devoted to the force exerted by small-amplitude, standing, solitary, and wind waves is contained in [2]. Investigation of the force exerted by bore type waves is at an early stage.

The present paper deals with bores formed upon rapid removal of a vertical shield which produces the initial free-surface level difference in a rectangular channel with an even horizontal bottom. In this model problem of full dam break, the kinematic characteristics of the waves have been studied well both theoretically and experimentally. In particular, the corresponding analytical solutions based on the first shallow-water approximation are given in [3, 4] and the results of a detailed experimental verification of these solutions are reported in [5, 6].

Bore impact on a vertical wall was studied in [7, 8], where bores were also generated by removal of a shield producing the initial free-surface level difference in a rectangular channel. However, the channel had an inclined bottom and a relatively small length. As a result, the kinematic characteristics of the bore in experiments [7, 8] differed from theoretical dependences [3, 4].

The main goal of the present study was to add to available experimental information on the force action of bore type waves. It is important that, in a certain time interval, the kinematic characteristics of the waves incident on an obstacle are accurately described by analytical solutions [3, 4]. Additional experimental data were also obtained on the effect of the free surface on the body drag under steady-state and unsteady conditions.

Kinematic Characteristics of Incident Waves. A diagram of the experiment, the basic notation, and the motionless coordinate system used are shown in Fig. 1. The dam-break problem splits into the cases of the initially dry ($h_+ = 0$) and flooded ($h_+ > 0$) tailwater bottom [4] (h_- and $h_+ < h_-$ are the initial headwater and tailwater depths of quiescent fluid, respectively). The wave propagation characteristics over a dry bottom differ significantly from those over a flooded bottom [5, 6]. In the present paper, the wave impact in the case of a dry bottom is not considered. A distinction is also made between the nonsubmerged and submerged states of head and tail conjugation after removal of the shield. According to theoretical studies [3, 4], the nonsubmerged state occurs at $h_+ < 0.138h_-$, which is confirmed by experiments [5, 6]. In the present paper, both states are considered.

The theoretical free-surface profile [3, 4] some time after removal of the shield is shown in Fig. 1. A level-depression wave propagates downstream, and a discontinuous wave propagates upstream. The following notation is used: c_0 is the propagation speed of the level-depression wave; D_1 is the propagation speed of the discontinuous

Lavrent'ev Institute of Hydrodynamics, Siberian Division, Russian Academy of Sciences, Novosibirsk 630090; bukreev@hydro.nsc.ru. Translated from Prikladnaya Mekhanika i Tekhnicheskaya Fizika, Vol. 49, No. 6, pp. 45–54, November–December, 2008. Original article submitted June 18, 2007; revision submitted August 15, 2007.

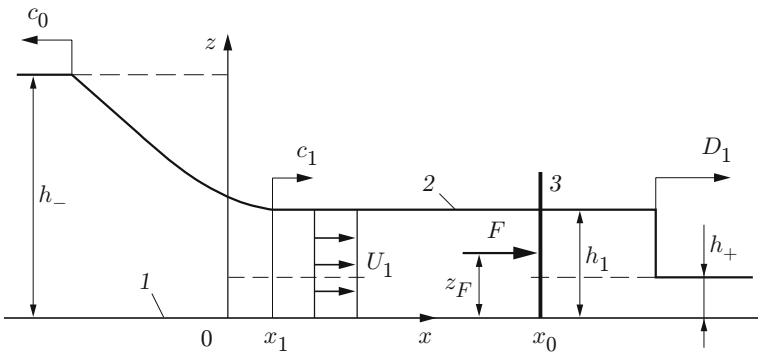

Fig. 1. Experimental setup: 1) channel bottom; 2) theoretical free-surface profile; 3) plate.

waves; h_1 and U_1 are the fluid depth and velocity behind the leading edge of the wave; c_1 is the propagation speed of the point at which the level-depression wave becomes the discontinuous wave. The theoretical wave profile depends only on the ratio x/t (the corresponding formulas are given in [3, 4]). If the length and width of the channel are infinite, the above-mentioned kinematic characteristics of the theoretical wave do not depend on time and are determined by three specified parameters of the problem: h_-, h_+, and the acceleration due to gravity g. These parameters can be integrated into only one dimensionless complex h_+/h_-. The free dimensional parameter g determines the characteristic velocity and time scales of the processes considered.

The longitudinal coordinate of the flow cross section at which the level-depression wave becomes the discontinuous wave is given by the relation $x_1 = c_1 t$ (see Fig. 1). If $x_1 > 0$, the state of head and tail conjugation is nonsubmerged, and if $x_1 < 0$, the state of head and tail conjugation is submerged. At $x_1 = 0$, the critical depth $h_* = 4h_-/9$ and the critical velocity $u_* = 2(gh_-)^{1/2}/3$ are established at the shield location. In the nonsubmerged and critical states, the specific discharge of the fluid moving downstream is $q = 8(gh_-)^{3/2}/27$ (per unit width of the channel), and its specific energy is $e = h_* + u_*^2/(2g) = 2h_-/3$ (per unit mass of the fluid).

Experimental and theoretical bores have a number of differences. At the leading edge of the theoretical bore, the fluid velocity, depth, and pressure change suddenly. In reality, the change of these parameters from one constant values to others occurs in the interval $\Delta x \approx 5(h_1 - h_+)$ [9]. There are five versions of the experimental bore [1] that differ, in particular, in the degree of development of undulations — gradually degenerating oscillations in the free-surface level behind the leading edge [10]. The degeneration of these nonlinear oscillations is due to the dispersion of gravitational waves. The first shallow-water approximation does not describe wave dispersion and undulations. The present experiments studied the force action of all versions of the experimental bore.

Experiments [6, 11, 12] have shown that the initial stage of the decay of the free-surface level discontinuity is not described in the classical first approximation of shallow-water theory; therefore, theoretical solutions [3, 4] are applicable only at a distance downstream of the shield location. In the present work, the value of x_0 was chosen large enough so that the parameters h_1, U_1, and D_1 differed from their experimental analogs by not more than 4%.

Experimental Technique and Result Processing. The experiments were performed in a rectangular channel of length 8.2 m, height 0.23 m, and width $B = 0.2$ m with an even horizontal bottom. The initial free-surface level difference $H = h_- - h_+$ was produced by a flat shield located at the channel cross section $x = 0$. At some time t, the shield was removed vertically upward. The lower edge of the shield left water in no more than 0.04 sec.

A vertical plate of width $b = 3$ cm and thickness $\delta = 0.4$ cm (see Fig. 1) was located in the tailwater at identical distances from the side walls of the channel and at a distance $x_0 = 1.4$ m downstream of the shield. In all experiments, the height of the plate exceeded the greatest height of fluid rise on the frontal face.

Generally, the hydrodynamic force acting on an obstacle has three components. The coordinates of the point of its application are unknown. In this work, only the longitudinal component of the force F and the vertical coordinate of the point of its application z_F were studied (see Fig. 1). The influence of the other components of the force was eliminated by suspending the plate in the manner shown schematically in Fig. 2.

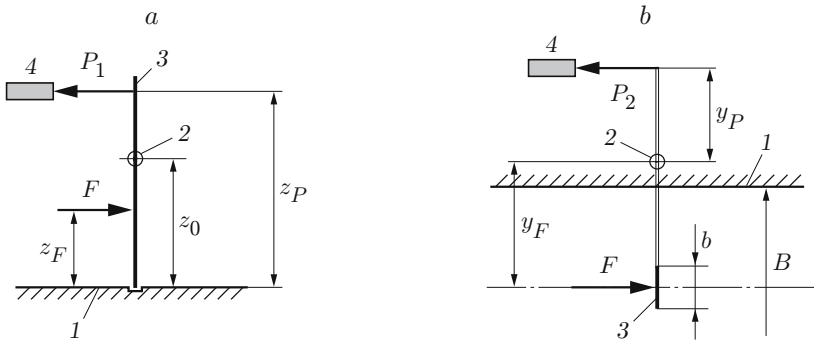

Fig. 2. Diagram of suspension of the plate: (a) suspension of the plate on a horizontal axis of rotation [channel bottom (1), axis of rotation (2), plate (3), and force transducer (4)]; (b) suspension of the plate on a vertical axis of rotation [side wall of the channel (1), axis of rotation (2), plate (3), and force transducer (4).

Figure 2a shows the section of the measuring system by the longitudinal plane of symmetry of the channel. In this case, the plate is suspended on the horizontal axis of rotation parallel to the y axis and has only one degree of freedom — rotation in the longitudinal direction which is prevented by the rigid force transducer. The parameters z_0 and z_P given in Fig. 2a are specified, and the force acting on the transducer P_1 is measured. The condition of equality of the moments of the forces with respect to the axis of rotation leads to the equation

$$(z_0 - z_F)F = (z_P - z_0)P_1, \tag{1}$$

which contains two unknown values F and z_F. Additional data can be obtained by three methods, in each of which experiments should be performed under the same conditions.

In the first method, two experiments are performed with only the coordinate z_0 being varied. If in the second experiment, $z_0 = z_{01}$, the transducer records the force P_{11}. Then, for F and z_F, we obtain the independent equation

$$(z_{01} - z_F)F = (z_P - z_{01})P_{11}.$$

In the second method, successive approximations are used to find the value of $z_0 = z_F$ at which the force acting on the transducer $P_1 = 0$.

In the third method, the force F is measured directly. The corresponding measuring system (top view) is shown in Fig. 2b. The plate is fixed on a vertical axis of rotation parallel to the coordinate axis z by means of a cantilever located above the channel. The axis of rotation is shifted transversely by a distance y_F relative to the vertical axis of symmetry of the plate, and the transducer is shifted by a distance y_P relative to the axis of rotation and measures the force P_2. The condition of equality of the moments of the forces with respect to the axis of rotation leads to

$$F = P_2 y_P / y_F. \tag{2}$$

In the present work, experimental data were obtained using Eqs. (1) and (2). All elements of the measuring system were outside the flow and did not cause additional perturbations. The other methods were used for control.

The force was measured by a Honeywell transducer with a linear static calibration characteristic and a natural frequency of about 100 kHz. The frequency characteristic of the entire measuring system is determined primarily by the natural frequency ω_0 and the damping decrement α of plate oscillations in the fluid. These parameters were determined as follows.

The plate placed in a quiescent fluid at a specified depth was subjected to a short-term impact. As a result, the impact pulse reached the input of the measuring system. We recorded the response of the system to this impact $Y(t)$, where t is time. This response is described by the function [13]

$$Y(t) = a \exp(-\alpha t) \sin(t\sqrt{\omega_0^2 - \alpha^2}).$$

The parameters ω_0 and α of the function $Y(t)$ depend on the depth of immersion of the plate in water. The values $\omega_0 = 80$ rad/sec and $\alpha = 2.9$ sec^{-1} were obtained under conditions of the greatest frequency distortions. Spectral

analysis of the forces showed that, for such values of ω_0 and α, the error due to frequency distortions, did not exceed 0.5%.

The depth of the flow incoming on the plate as a function of time $h(t)$ was measured by wavemeters using the technique described in [6]. The frequency characteristics of the wavemeters were determined from their sinusoidal oscillations in the quiescent fluid at various frequencies. For the wavemeters, the values $\omega_0 = 36$ rad/sec and $\alpha = 22$ sec^{-1} were obtained. Spectral analysis of the incident waves showed that the wavemeters did not cause frequency distortions.

In the absence of the plate, the fluid flow velocity $u(z,t)$ at $x = x_0$ and $y = 0$ was measured by the so-called PIV method using Dantec Dynamics equipment. We will further use information only on the time-independent velocity U_{as} averaged over z at a distance behind the leading edge of the bore at which the flow is steady-state.

Generally, the parameters F and z_F (see Fig. 1) depend on t, x_0, B, h_-, h_+, b, g, the density ρ, and the dynamic fluid viscosity μ. If the parameters h_-, g, and ρ are used as characteristic scales, then in experiments, the examined functions F and z_F will depend on the following dimensionless arguments:

$$\tau = t\Big(\frac{g}{h_-}\Big)^{1/2}, \quad x^0 = \frac{x}{h_-}, \quad B^0 = \frac{B}{h_-}, \quad h_+^0 = \frac{h_+}{h_-}, \quad b^0 = \frac{b}{h_-}, \quad \mathbf{Re} = \frac{g^{1/2}H^{3/2}}{\nu}.$$

Here $\nu = \mu/\rho$ is the kinematic viscosity; **Re** is the Reynolds similarity criterion determined using the specified initial level difference H and the characteristic initial fluid velocity $V = (gH)^{1/2}$. Below, we will use the dimensionless complex $\text{Re} = Ub/\nu$. In addition to the specified parameters b and ν, it contains the incoming-flow velocity U, which also depends on the specified parameters, in particular, the similarity criterion **Re**. Complexes of this type are called numbers. In our case, the complex Re is the Reynolds number.

In the problem considered, the set of similarity criteria is interesting in that it contains only one element **Re** dependent on fluid viscosity. In the cases where the viscosity effect can be ignored, the results of laboratory experiments can be extended to full-scale conditions with only geometrical similarity taken into account. Experiments [5, 6] have shown that for the kinematic characteristics of the waves considered, this is valid for $B/H > 0.8$ and $\mathbf{Re} > 3.5 \cdot 10^4$. In the present work, these conditions are satisfied.

As regards the influence of fluid viscosity on the force action of the waves, we note the following. In the case of unbounded steady-state flow over a body, the expression for the total drag includes two terms: the friction drag due to viscosity and the vortex drag dependent on the body shape. For a plate, the second term is much larger than the first [14]. In the case of unsteady flow, one more term dependent only on the inertia of the incoming flow is added. The assumption of a weak influence of viscosity on the drag force at large Reynolds numbers is indirectly supported in the present work.

Results of Experiments. Figure 3 shows the profiles of the waves incident on the plate recorded by a motionless wavemeter located at the section $x = x_0$ [$t^0 = (t - t_0)(g/h_-)^{1/2}$, $h^0 = h/h_1$ $h_+^0 = h_+/h_-$, where t_0 is the reference time chosen arbitrarily and different in different cases]. Some time after the removal of the shield, the wavemeter records a constant value of the initial tailwater depth. An increase in the depth is observed beginning at the moment the wave arrives at the point $x = x_0$.

In Fig. 3, it is evident that the head of the waves considered differs from the head of the theoretical wave shown in Fig. 1. However, the fluid depth reaches a constant value h_{as}^0. In theoretical studies [3, 4], the same parameter was the constant depth $h_1^0 = h_1/h_-$ which was established instantaneously and depended only on the parameter $h_+^0 = h_+/h_-$. Curve 1 in Fig. 3 refers to the range of values of h_+^0 for which the wave head has the form of a classical hydraulic jump with a developed roller and negligibly small undulations. Curve 2 in Fig. 3 refers to the value of h_+^0 for which undulations prevail and the roller at the leading edge is developed only slightly. Above a certain value h_+^0, the waves take the form of a smooth undular bore (curve 3 in Fig. 3).

Figure 4 shows the dimensionless force $F^0 = 2F/(\rho g b h_-^2)$ versus t^0. The time reference is arbitrary. After the passage of the wave head, the force reaches the constant value F_{as} dependent on h_+^0. During the time of existence of unsteady flow, the behavior of the force is determined by the form of the incident-wave head. If the head has the form of a hydraulic jump with a developed roller (curve 1 in Fig. 3), the force reaches a constant value after irregular fluctuations (curve 1 in Fig. 4). If the incident wave is dominated by undulations (curves 2 and 3 in Fig. 3), the fluctuations of the force have a regular nature and follows in frequency the depth variation (curves 2 and 3 in Fig. 4).

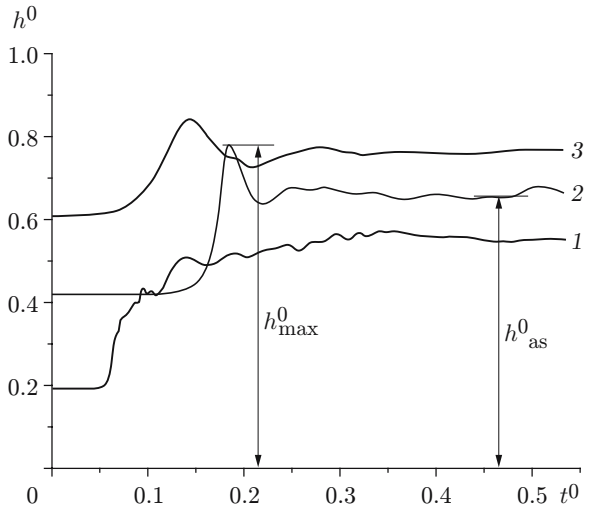

Fig. 3

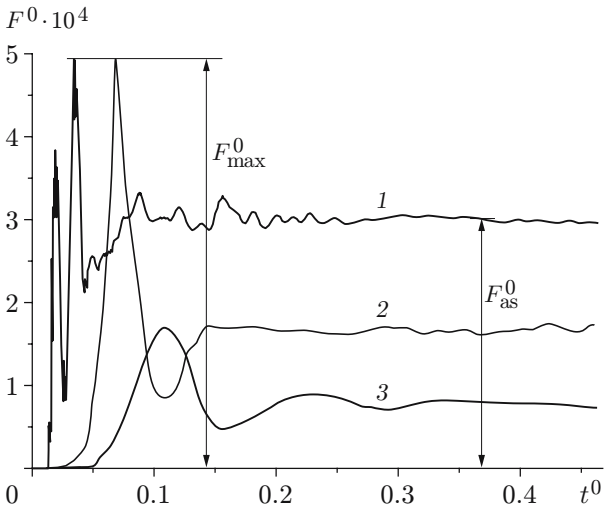

Fig. 4

Fig. 3. Results of depth measurements at $h^0_+ = 0.186$ (1), 0.419 (2), and 0.605 (3).

Fig. 4. Results of force measurements at $h^0_+ = 0.186$ (1), 0.419 (2), and 0.605 (3).

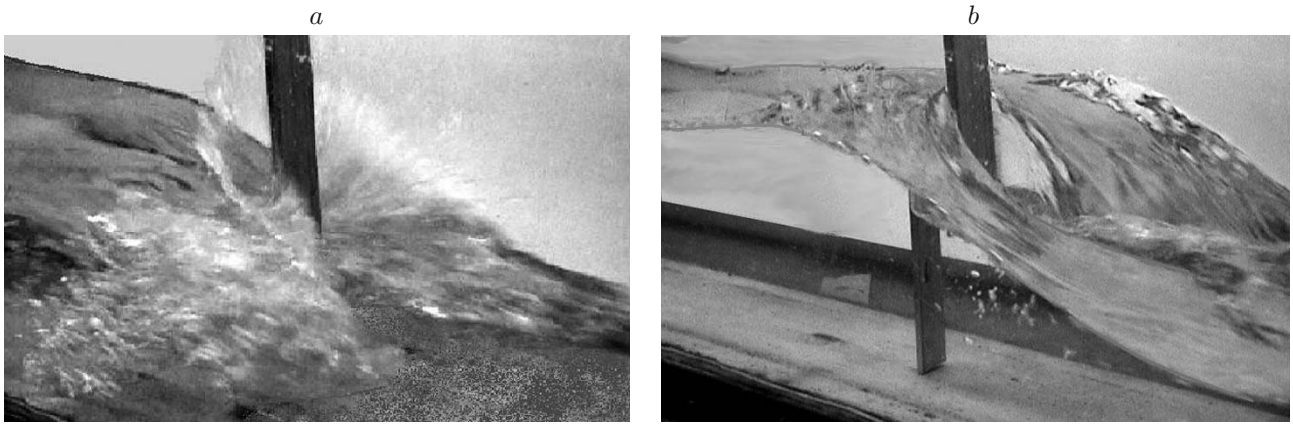

Fig. 5. Flow over the plate at $h^0_+ = 0.186$: (a) initial stage; (b) steady-state regime.

The flow pattern over the plate is presented in Fig. 5. Figure 5a corresponds to the time when the bore with a developed head roller begins to flow over the plate, and Fig. 5b to the moment when the force reaches the asymptotic value.

On the frontal face of the plate, the free-surface level increases, and on the rear face it decreases, resulting in generation of waves similar to ship waves. In the vicinity of the plate, oblique waves prevail. The level depression is also retained at some distance downstream of the plate in an internal region bounded by oblique waves. Further, the free-surface level is almost restored to its value at a large distance upstream, and the waves become weak.

Figure 6 shows curves of the asymptotic F_{as} and maximum $F_{\max}$ forces versus the parameter h^0_+ (for better illustration, the force are presented in dimensional form). The experimental points were obtained by the method described above, in which F was measured separately from z_F [see Fig. 2b and formula (2)]. The dimensionless coefficients of the forces are considered below.

Curves of the coordinate of the point of application of the force on h^0_+ are given in Fig. 7 [$h^0_{0.5} = h_1/(2h_-)$ is the dimensionless half of the depth h_1 behind the theoretical wave front; z^0_{as} and $z^0_{\max}$ are the experimental coordinates of the points of application of the forces F_{as} and $F_{\max}$ normalized by h_-]. Curve 1 is calculated using the algorithms given in [4], and curves 2 and 3 are obtained using formula (1). The force F was specified by analytical

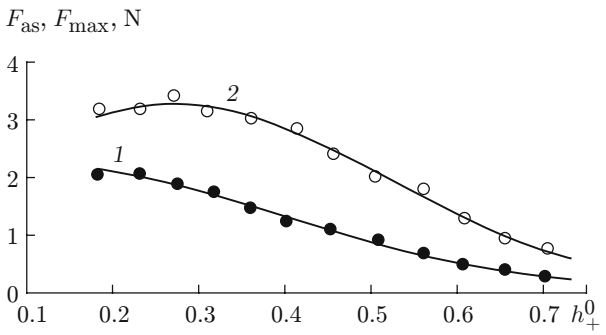

Fig. 6

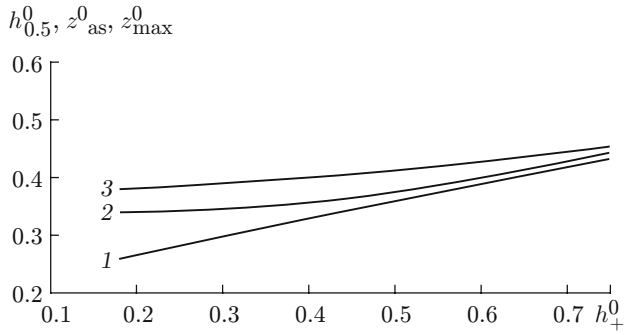

Fig. 7

Fig. 6. Asymptotic (1) and maximum (2) forces versus parameter h_+^0: points correspond to the experiment, and curves to the results of approximation by the Gauss function of errors.

Fig. 7. Theoretical depth of the incoming flow (1) and the vertical coordinates of the points of application of the asymptotic (2) and maximum (3) forces versus parameter h_+^0.

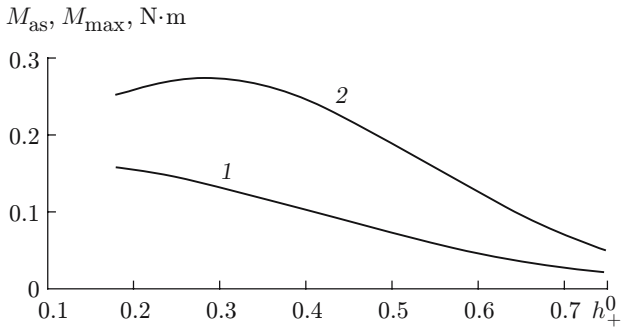

Fig. 8. Asymptotic (1) and maximum (2) overturning moments versus parameter h_+^0.

expressions corresponding to curves 1 or 2 in Fig. 6. The force P_1 in the computation formula (1) was measured in a repeated series of experiments using the setup shown schematically in Fig. 2a. The values of the force P_1 obtained by approximation of experimental data by the Gauss error function were substituted into formula (2).

In Fig. 7, it is evident that the point of application of the force is above the half-depth of steady-state incoming flow established at a large distance from the leading edge of the bore. This agrees with the features of the free-surface flow over the plate (see Fig. 5).

The analytical dependences obtained by the approximation were used to calculate the characteristic values of the overturning moment acting on the cylinder $M_{as} = F_{as} z_{as}$ and $M_{max} = F_{max} z_{max}$ (see Fig. 8).

In the case of steady-state flow, the drag force of the plate F_s is represented in the following form [2, 14]:

$$F_s = C_s \rho b l U^2/2.$$

Here U is the incoming-flow velocity, l and b are the length and width of the plate, and C_s is the dimensionless drag coefficient. If the incoming flow is unsteady, at least two coefficients are used, as, for example, in the Morison formula [2]:

$$F_n = \frac{C_s \rho b l |U| U}{2} + C_n \rho \frac{\pi b^2 l}{4} \frac{\partial U}{\partial t},$$

where F_n is the unsteady drag force and C_n is the coefficient characterizing the inertia of the incoming flow.

In unbounded incompressible fluid flow, the coefficients C_s and C_n depend on time, the relative plate length l/b, the Reynolds number $\mathrm{Re} = Ub/\nu$, and the Strouhal number $\mathrm{Sh} = UT/b$ (T is the characteristic time scale). The presence of the free surface significantly complicates the problem. In this case, it is necessary to take

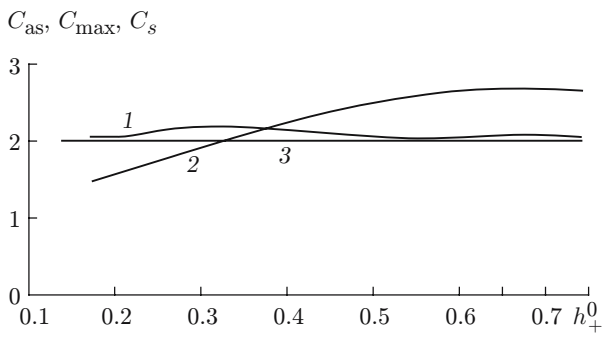

Fig. 9

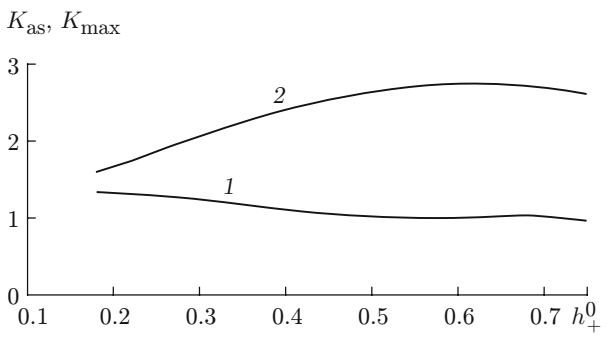

Fig. 10

Fig. 9. Coefficients of the forces versus parameter h_+^0: curves 1, 2, and 3 refer to C_{as}, $C_{\max}$, and C_s, respectively.

Fig. 10. Coefficients of the overturning moments versus parameter h_+^0: curves 1 and 2 refer to K_{as} and $K_{\max}$, respectively.

into account the influence of the Froude number $\text{Fr} = U^2/(gh)$ (h is the incoming-flow depth) and the fact that the parameters U, T, and $h = l$ depend on the type of waves.

Bearing in mind that unsteady flow occurs only at the relatively short head of bore waves, we introduce the following time-independent coefficients to make the forces and the overturning moments dimensionless:

$$C_{\text{as}} = \frac{2F_{\text{as}}}{\rho b h_1 U_1^2}, \qquad C_{\max} = \frac{F_{\max}}{F_{\text{as}}}, \qquad K_{\text{as}} = \frac{2M_{\text{as}}}{\rho b h_1^2 U_1^2}, \qquad K_{\max} = \frac{M_{\max}}{M_{\text{as}}}.$$

The first of these coefficients, which is similar to the standard drag coefficient C_s, uses the fluid depth and velocity in the time interval in which the incoming flow is steady-state. The remaining coefficients are specific to the problem considered. In particular, the last two coefficients are meaningful only for the overturning moment with respect to the channel bottom.

The definitions of the above coefficients use the theoretical quantities h_1 and U_1, which, as noted above, are slightly different from the experimental quantities h_{as} and U_{as}. The differences between the theoretical and experimental depths and velocities are allowed for in empirical coefficients for the forces and moments.

Figures 9 and 10 show experimental curves of the coefficients of the forces and the overturning moments versus the parameter h_+^0 in the following ranges of other parameters: $0.021 \leqslant \text{Fr} = U_1^2/(gh_1) \leqslant 0.700$, $3.5 \leqslant h_1/b \leqslant 6.3$, and $3.8 \cdot 10^4 \leqslant \text{Re} = bU_1/\nu \leqslant 9.5 \cdot 10^4$. Curve 3 in Fig. 9 corresponds to the value of the drag coefficient of the plate in unbounded steady-state flow $C_s = 2$ [14]. The data in Fig. 9 show that, in the asymptotic regime, the drag coefficient of the plate C_{as} slightly exceeds the drag coefficient C_s in the case of unbounded steady-state flow. In addition, the coefficient C_{as} depends weakly on h_+^0, and hence, on the Reynolds number Re and the Froude number Fr, which, in the problem considered are uniquely related to h_+^0.

In free-surface flow, the total drag is due to forces of the viscous, vortex, and wave natures. The weak dependence of the coefficient C_{as} on Re is a consequence of the weak influence of fluid viscosity, and the weak dependence on Fr indicates that an increase in the wave drag is accompanied by almost the same decrease in the drag due to the pressure gradient on the frontal and rear faces of the plate. The wave drag is determined by the free-surface level difference on the plate (see Fig. 5): the larger the difference , the greater the wave drag. However, in this case, part of the rear face of the plate is in air, resulting in a decrease in the pressure difference on the frontal and rear faces compared to the case of unbounded flow.

Conclusions. The experimental data obtained show that the maximum value of the force can exceed its asymptotic value by a factor of 2.7 (see Fig. 9). A significant excess is observed in the range of h_+^0, in which the incident wave has the form of a smooth undular bore. However, one should take into account that in this range of h_+^0, the values of the forces (see Fig. 6) are relatively small. The most significant force is exerted by a bore with a developed head roller. A similar result is obtained for the overturning moments (see Figs. 8 and 10).

This work was supported by the Russian Foundation for Basic Research (Grant No. 07-01-00015) and Integration Project of the Russian Academy of Sciences No. 4.14.1.

REFERENCES

1. Ven Te Chow, *Open-Channel Hydraulics*, McGraw Hill, New York (1959).
2. G. Moberg, "Wave forces on a vertical slender cylinder," Report Ser. A:16, Göteborg, Calmers Univ. of Technology (1988).
3. S. A. Khristianovich, S. G. Mikhlin, and B. B. Devison, "Unsteady motion in channels and rivers," in: *Some New Problems of Continuum Mechanics* [in Russian], Izd. Akad. Nauk SSSR (1938), pp. 15–154.
4. J. J. Stoker, *Water Waves*, Wiley, New York (1957).
5. R. F. Dressler, "Hydraulic drag effect upon the dam-break function," *J. Res. Nat. Bur. Stand*, **49**, No. 3, 217–225 (1952).
6. V. I. Bukreev, A. V. Gusev, A. A. Malysheva, and I. A. Malysheva, "Experimental verification of the gas-hydraulic analogy by the example of the dam-break problem," *Izv. Ross. Akad. Nauk, Mekh. Zhidk. Gaza*, No. 5, pp. 143–152 (2004).
7. P. Scotton, "Dynamic impact of Debris flows: Experimental study," Preprint, Univ. di Trento, Trento (1996).
8. F. Trivellato and P. Scotton, "Bore impact upon a wall (experimental data base)," Preprint, Univ. Degli Studio di Trento, Trento (2001).
9. P. G. Kiselev, *Handbook on Hydraulic Calculations* [in Russian], Gosenergoizdat, Moscow–Leningrad (1957).
10. H. Favre, *Etude Théorique et Expérimentale des Ondes de Translation Dans les Canaux Découvertes*, Dunod, Paris (1935).
11. P. K. Stansby, A. Chegini, and T. C. D. Barnes, "The initial stages of dam-break flow," *J. Fluid Mech.*, **374**, 407–424 (1998).
12. V. I. Bukreev amd A. V. Gusev, "Initial stage of generation of dam-break waves," *Dokl. Akad. Nauk Ross. Akad. Nauk*, **401**, No. 5, 1–4 (2005).
13. Ya. G. Panovko, *Foundations of the Applied Theory of Oscillations and Impact* [in Russian], Mashinostroenie, Leningrad (1976).
14. J. Daily and D. R. F. Harleman, *Fluid Dynamics*, Addison–Wesley, Ontario (1966).